AeroChem TN-206

DOE/JPL 954862-79/6

Distribution Category UC-63

DEVELOPMENT OF A MODEL AND COMPUTER CODE TO DESCRIBE SOLAR GRADE SILICON PRODUCTION PROCESSES

SIXTH QUARTERLY REPORT

R. SRIVASTAVA AND R.K. GOULD

MAY 1979

The JPL Low-Cost Solar Array Project is sponsored by the U. S. Department of Energy and forms part of the Solar Photovoltaic Conversion Program to initiate a major effort toward the development of low-cost solar arrays. This work was performed for the Jet Propulsion Laboratory, California Institute of Technology by agreement between NASA and DoE.

AeroChem Research Laboratories, Inc.

Princeton, New Jersey

AeroChem TN-206

DOE/JPL 954862-79/6
Distribution Category UC-63

DEVELOPMENT OF A MODEL AND COMPUTER CODE TO DESCRIBE SOLAR GRADE SILICON PRODUCTION PROCESSES

SIXTH QUARTERLY REPORT

R. SRIVASTAVA AND R. K. GOULD

MAY 1979

JPL Contract No. 954862
DRL Item No. 4, DRD No. QR
LSA Silicon Material Task

Approved by _____
Hartwell F. Calcote
Director of Research

AeroChem Research Laboratories, Inc.
Princeton, New Jersey

FOREWORD AND ACKNOWLEDGMENTS

This report covers the period 1 January 1979 to 31 March 1979. During this period, D.B. Olson and P.J. Howard contributed to the program.

ABSTRACT

This program aims at developing mathematical models and computer codes based on these models, which allow prediction of the product distribution in chemical reactors for converting gaseous silicon compounds to condensed-phase silicon. The major interest is in collecting silicon as a liquid on the reactor walls and other collection surfaces. Two reactor systems are of major interest, the Westinghouse $SiCl_4$/Na reactor in which Si(ℓ) is collected on the flow tube reactor walls and the new AeroChem reactor in which Si(ℓ) droplets formed by the $SiCl_4$/Na reaction are collected by a jet impingement method.

During this quarter the following tasks have been accomplished: (i) formulation of a model for silicon vapor separation/collection from the developing turbulent flow stream within reactors of the Westinghouse type, (ii) modification of an available general parabolic code to achieve solutions to the governing partial differential equations (boundary layer type) which describe migration of the vapor to the reactor walls, (iii) a parametric study using the boundary layer code to optimize the performance characteristics of the Westinghouse reactor, (iv) calculations relating to the collection efficiency of the new AeroChem reactor, and (v) final testing of the modified LAPP code for use as a method of predicting Si(ℓ) droplet sizes in these reactors.

TABLE OF CONTENTS

LIST OF TABLES

LIST OF ILLUSTRATIONS

I. INTRODUCTION

The goal of this program is to develop mathematical models and computer codes that will predict product distribution in chemical reactors designed to convert gaseous silicon compounds to condensed-phase silicon. Emphasis is placed on collecting silicon as a liquid on the reactor walls and other collection surfaces. The two reactor systems being studied are the Westinghouse $SiCl_4/Na$ reactor[1] in which Si(ℓ) is collected on the flow tube reactor walls, and the new AeroChem reactor in which Si(ℓ) droplets formed by the $SiCl_4/Na$ reaction are collected by a jet impingement method.[2]

Conceptually, it is useful to visualize a flow reactor of the Westinghouse type[1] as having two distinct parts:

(i) An "upstream"section in which gaseous silicon halide (e.g., $SiCl_4$), with argon and hydrogen as diluents, entrains into a jet of sodium vapor, mixes rapidly due to turbulence, and reacts to yield the required silicon-containing product gas stream.

(ii) A "downstream" section, with cooled reactor walls ($\approx$ 1700 K), through which the hot ($\approx$ 3500 K) developing flow of product gases passes. Separation (and collection) of silicon occurs in this section by the passage of condensed silicon droplets and uncondensed vapor, through the turbulent boundary layers onto the reactor walls.

The situation is depicted in Fig. 1. Because of the difficult nature of both problems, our analysis also has two distinct parts.

The first part of the analytical work, using LAPP (AeroChem's rocket plume code), considers the problem of the open, turbulent, axisymmetric jet with finite rate, multiple-step chemical reactions. Recent modifications of LAPP have extended its capabilities to include a detailed kinetic description of silicon droplet formation via homogeneous nucleation and hence can be used to compute the streamwise histories of droplet size and number concentration along the reactor.* On the other hand, the silicon separation/collection problem in the "downstream" section is dominated by the presence of walls and is better

---

* Test runs are currently being made and the modified code is nearly debugged. The solutions from LAPP will be an important input in the solution of the "downstream" problem.

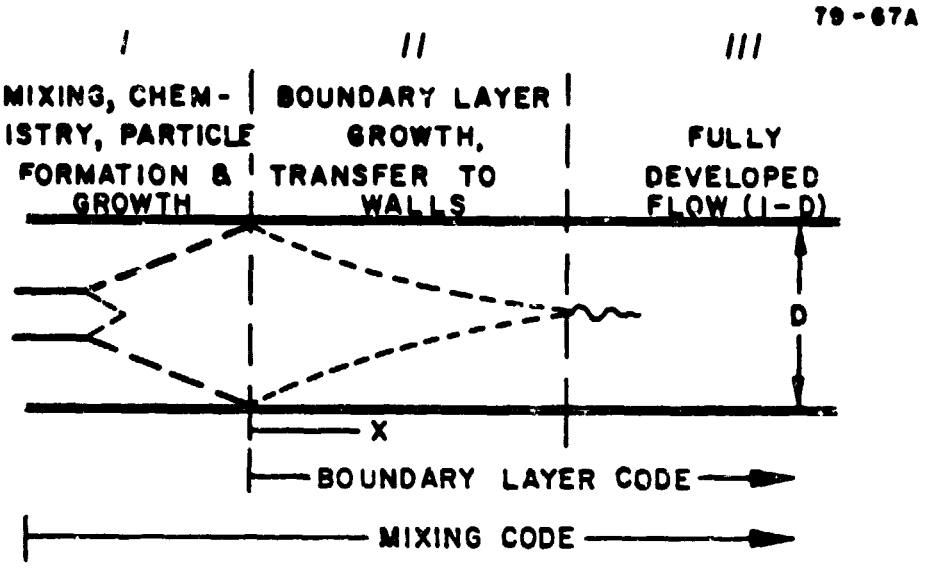

FIGURE 1. SCHEMATIC OF THE VARIOUS REGIMES WITHIN A SILICON REACTOR

handled with the well-known GENMIX (Version 4A) computer program[3] for the solution of boundary layer type (i.e., parabolic) problems. This latter problem is the major subject of discussion in this report.

II. WALL DEPOSITION OF SILICON

The case of silicon vapor deposition, caused by the various convective-diffusion processes in the developing, turbulent flow field encountered over most of the "downstream" reactor section, is analyzed here using operating conditions typical of the current Westinghouse reactor design.[1] Existing Westinghouse analyses[1] of the silicon separation/collection problem use the following rather simple model. By considering a differential axial segment of the flow as a control volume, these analyses express mass, momentum, and energy balances in terms of the net efflux of these quantities across the control volume boundaries. The details of the boundary layer structure near the reactor walls are ignored by the utilization of empirical heat and mass transfer coefficients (Nusselt numbers), appropriate to a given developing

turbulent pipe flow. In particular, the streamwise variation of the Nusselt number (for given Reynolds and Prandtl numbers) is taken from the experimental results of Boelter et al,[4] pertaining to the case of air flowing through a pipe with a right-angle bend entrance. Furthermore, the effects of condensation on the wall heat and mass transfer rates are accounted for via a correction factor based on a fully-developed (i.e., no streamwise variations in flow properties) turbulent pipe flow analysis involving silicon vapor (no droplets). Thus condensation is treated solely as an augmenter of heat and mass fluxes. Using this one-dimensional, constant property analysis it was concluded that the silicon vapor collection efficiency of the proposed 8 m long reactor would be about 80%.

Thus, while the Westinghouse analysis outlined above serves as a useful tool for preliminary reactor design, a unified analysis (such as the one we adopt) will ultimately be needed to make reliable design predictions. A proper consideration of the dominant deposition mechanisms and the structure of the developing turbulent boundary layer is essential before measures can be taken to improve the silicon collection efficiency of a given reactor. In what follows we discuss exactly such a model for the case of silicon vapor deposition. Undoubtedly, the presence of condensing silicon droplets in the developing turbulent flow field will alter the silicon collection efficiency since the turbulent, Soret, and Brownian diffusional behavior of particles can differ greatly from that of vapor molecules.[5] This latter aspect of the problem will be the subject of future reports.[6-8] Finally, it might be worth mentioning that when the details of the silicon deposition behavior are adequately modeled and computerized (as we have done) they will enable the designer to produce an optimum reactor design with minimum experimental effort.

III. SILICON VAPOR DEPOSITION/COLLECTION MODEL

We start with the assumption that all chemical reactions have reached completion, and hence the product gas stream is chemically inert, just prior to entering the downstream section (region II, Fig. 1) of the reactor. Thus, in this section the model formulated will describe the behavior of the various convection and diffusion processes responsible for depositing silicon on the reactor walls. The physical problem involves an analysis of the hot, turbulent,

developing flow field within a circular pipe with cooled walls. Due to the large temperature variation between the reactor core flow and the walls, it is essential to include the effects of non-uniform fluid properties and the possible formation of silicon droplets due to condensation (caused by cooling silicon vapor). However, for simplicity, in the present analysis we restrict attention to the case with no condensation. That is, silicon is assumed to exist only in the vapor state.

Yet another simplification is rendered in this analysis by viewing the overall product gas mixture as an effective binary system, with silicon as one species and all other gases (mainly NaCl, Ar, H_2) as the only other species (referred to subsequently as the "carrier" gas). The molecular weight and other properties of the carrier gas are taken to be a weighted average of the properties of the individual components. On this basis, the diffusional behavior of silicon vapor through the surrounding gas can be uniquely described in terms of the appropriate mass diffusivities (or mass transport coefficients).[5] On the other hand, the thermal diffusivity (or heat transport coefficient) of the overall product gas mixture will be nearly equal to that of the carrier gas alone, since silicon concentrations are typically low. In the case of silicon vapor deposition, the relative importance of heat and mass transfer processes inside a typical reactor is nearly equal. That is, the Lewis number for the system is close to unity. The effect of turbulence, as treated in the model considered, lies mainly in enhancing the diffusive transport of heat, mass, and momentum.* The enhancement due to the so-called turbulent counterparts of the abovementioned diffusivities will be assumed to be such that the "effective Lewis number" remains close to unity. That is, turbulence enhances heat and mass transfer rates equally. However, according to current belief and experimental data the enhancement of momentum transfer rates due to turbulence is somewhat less (a fact represented by setting the turbulent Prandtl number† equal to 0.9).

---

* The diffusive transport of momentum (or vorticity) is analogously controlled by the kinematic viscosity (ν), or momentum diffusivity.

† The Prandtl number is the ratio of momentum diffusivity to thermal diffusivity.

It is clear, therefore, that a good description of turbulent transport coefficients is pivotal to the success of the present model. For now, a mixing length approach to turbulence modeling has been adopted. The chief drawback of this approach is that it relies heavily on an empirical determination of several constants, some of which might vary from one flow situation to another. This handicap will have to be overcome by the use of more sophisticated (differential) models of turbulence. This latter class of turbulence models, which describe the mixing length via differential equations (rather than algebraic ones, as done here), can, of course, be blended into the present formulation. However, we believe that since turbulent heat/mass transfer predictions using even the most elaborate approaches sometimes incur errors of up to 15%,[9] retaining the mixing length model would at least give us the advantage of greater simplicity with relatively little loss of achievable accuracy. Moreover, the mixing length model has been extensively studied and tested in pipe flow configurations against both experimental data[3] and the predictions of more sophisticated models.[10,11]

In view of the abovementioned assumptions and recognizing that the developing pipe flow processes of interest are characterized by comparable changes in the radial and axial directions (i.e., two-dimensional, axisymmetric) one may adopt the Patankar and Spalding[3] turbulent boundary layer formulation for the conservation of overall mass, momentum, energy (or stagnation enthalpy) and silicon vapor species.* No attempt will be made to reproduce these well-established parabolic, partial differential equations here since they have been fully detailed in Refs. 3 and 12. Instead here we choose to discuss aspects not immediately obvious from their discussion.

A. THE PATANKAR-SPALDING FORMULATION

Implicit in the governing equations used by these authors[3,12] are the following assumptions:

---

* It can be estimated from the magnitudes of the various diffusivities that the velocity, temperature, and species boundary layers will all develop at nearly the same rate. The "fully-developed" state is not reached until some 40-60 diam downstream from the pipe inlet.

(i) The density fluctuations caused by turbulence are of insignificant importance compared to the flux contributions of other fluctuating quantities (e.g., velocity, temperature, concentration).

(ii) The dissipation rate of turbulent kinetic energy (due to velocity fluctuations interacting with the mean velocity) is negligible compared to the viscous dissipation rate of mean kinetic energy.

Under these assumptions, it is possible to reduce the otherwise complicated turbulent boundary layer equations to a form similar to the better-understood steady, compressible, laminar boundary layer equations, provided one defines suitable "effective" values for the momentum, thermal, and mass diffusivities discussed earlier. These have been defined by the following flux-gradient relationships (assuming Newtonian behavior):

$$\tau \equiv \mu_{eff} \frac{\partial u}{\partial y} \qquad \text{(shear stress)}$$

$$q'' \equiv -\Gamma_{h,eff} C_p \frac{\partial T}{\partial y} \qquad \text{(heat flux)}$$

$$j_i'' \equiv -\Gamma_{i,eff} \frac{\partial Y_i}{\partial y} \qquad \text{(mass flux of species i)}$$

where μ_{eff} is the effective viscosity, $\Gamma_{h,eff}$ the ratio of effective thermal conductivity (λ_{eff}) to the constant pressure specific heat of the carrier gas (C_p), and $\Gamma_{i,eff}$ the product of the mean gas density (ρ) and the effective mass diffusivity ($D_{i,eff}$) of silicon vapor in the carrier gas. u, T, and Y_i denote the time-averaged streamwise velocity, absolute temperature, and mass fraction of silicon, respectively.

Each of the effective transport coefficients above is the sum of a laminar (or molecular) contribution and a pseudo, turbulence-induced contribution. The latter may be greater by some two orders of magnitude in fully turbulent (i.e., nearly inviscid) regions, such as the reactor core flow. However, closer to the reactor walls turbulence energy is rapidly depleted due to the dissipating influence of molecular viscosity, and transport is affected mainly by the laminar (molecular) mechanism. As a result the turbulent parts of the transport coefficients can vary significantly across

the reactor cross-section. The motivation for introducing a "mixing-length," or any other turbulence model, is to describe this variation realistically.

In the present analysis the following radial variation of mixing length, from the reactor axis (or centerline) to the wall, was prescribed:

$$\ell = \begin{cases} \lambda\delta \quad , \quad y > \dfrac{\lambda\delta}{K} & \text{(core layer region)} \\ Ky[1-\exp(-y^+/A^+)], \quad 0 \leq y \leq \dfrac{\lambda\delta}{K} & \text{(near wall region)} \end{cases}$$

where y is the distance from the wall, δ is the thickness of the turbulent boundary layer, and λ, K, and A^+[†] are taken to have the constant values 0.09, 0.435, and 26.0, respectively. Physically, such a distribution of mixing length distinguishes regions of high local Reynolds number, $y^+ \equiv yu_*/\nu$,[‡] (or nearly inviscid flow) from those regions near the wall which are governed by the progressively increasing effect of molecular viscosity (i.e., a "damping" of the mixing length with decreasing y^+, according to Van Driest's[14] exponential law). Note that this permits a viscous sublayer region next to the reactor walls so that the influence of even weak turbulent fluctuations is felt. Just outside the viscous sublayer the mixing length obeys an undamped, "defect law" behavior (i.e., $\ell = Ky$).

Using the above mixing length distribution it is possible to express the effective viscosity as:

$$\mu_{eff} = \mu_{turbulent} + \mu_{laminar}$$

$$= \rho\ell^2\left|\frac{\partial u}{\partial y}\right| + \mu$$

---

† It has been shown[13] more recently that A^+ is a sensitive function of pressure gradient and wall blowing or suction. This parameter determines the thickness of the "viscous sublayer" egion.

‡ u_* is the so-called "friction velocity" defined here in terms of the local shear stress by the relation $u_* \equiv (\tau/\rho)^{1/2}$

where $|\frac{\partial u}{\partial y}|$ is the magnitude of the time-averaged velocity gradient normal to the reactor wall. Since this quantity decreases away from the wall (becoming zero at the boundary layer edge) turbulence is operative only in regions in which the velocity gradient exceeds a small critical value. If, in any flow region the turbulence velocity scale $|\ell \frac{\partial u}{\partial y}|$ falls below a certain fraction of the local velocity, this quantity is set to the local prevailing velocity. Such a circumstance tends to occur in the fully-turbulent core flow region of the reactor.

B. COMMENTS ON THE NUMERICAL SOLUTION PROCEDURE

Since the governing equations to be solved are parabolic partial differential equations, their solution requires the specification of appropriate initial and boundary conditions. In the present study the initial conditions at the pipe entrance were specified as uniform (corresponding to centerline values) profiles of u, T, and Y_i across the pipe cross-section. The domain of integration was taken to be the region between the pipe centerline and the wall. Boundary conditions on u, T, and Y_i were specified at the wall as:

$$u = 0$$

$$T = T_w(\text{constant}) = 1700 \text{ K}$$

$$Y_i = Be^{-A/T_w} \approx 0^*$$

The last condition is a consequence of assuming that silicon vapor is in equilibrium at the wall (i.e., the partial pressure equals the saturated vapor pressure). The centerline boundary conditions on these variables were taken to correspond to the symmetry conditions:

$$\frac{\partial u}{\partial y} = 0, \quad \frac{\partial T}{\partial y} = 0, \quad \frac{\partial Y_i}{\partial y} = 0$$

---

* A and B are constants with the values 46710.0 K and 7.3166×10^{10} N m^{-2}, respectively.

Using the above initial and boundary conditions, GENMIX produced solutions at specific downstream stations along the reactor by marching forward in steps (whose size was proportional to the local boundary layer thickness). At each step the solution to the coupled system of conservation equations is carried out using a fully implicit, 6-point, finite difference algorithm (based on an integral approach that ensures conservation, rather than the usual Taylor series expansion). The algorithm uses a substitution method for solving the resulting system of coupled algebraic equations (with a tri-diagonal matrix), thus avoiding the time-consuming and unreliable operation of inverting the coefficient matrix. It was found in this study, as in others, that GENMIX is extremely efficient as a code. For instance, the full solution for a 9 m reactor length with some 80 to 100 radial grid points is completed in about 17 s (CP time on CDC 7600 computer).

The remarkable efficiency of GENMIX is really a result of the many different time-saving features built into the code. While the program chooses its own forward marching step size, the cross-stream grid spacing is specified as input. In the present problem, the grid points were so chosen as to be unequally spaced over the pipe radius, with a greater resolution capability near the wall, where gradients were steep. Furthermore, it must be noted that the solution in GENMIX is not carried out in physical space (x,y) but rather in the transformed von Mises[15] coordinates (x,ω). In this latter coordinate system, the normalized stream function ω always provides a fixed integration domain: $0 \leq \omega \leq 1$. In general, the advantage of working in this transformed space is the greater solution accuracy and ease that results from imposing boundary conditions at fixed extremities. However, in the solution of constant radii pipe flows (such as the present case), this advantage is not fully realized since the two extremities remain fixed even in physical space. Of course, an alternative solution tactic may have been to solve the problem between the wall and the edge of the developing boundary layer. In this latter case, working in the transformed stream function ordinates may be a definite advantage.

A major disadvantage of the GENMIX solution procedure may be its handling of the near-wall flow. The reactor wall is a point of singularity in the (x,ω) space because the flow velocity there is zero and it multiplies the highest derivatives of the transformed equations. This disconcerting feature also tends to render the transformation process back to physical space somewhat

inaccurate for grid points close to the wall. In order to circumvent some of the difficulties associated with this singlar point, the Patankar-Spalding procedure generates solutions for the region next to the wall using a turbulent Couette flow analysis (further simplified using a constant property assumption). Thus one does not obtain a rigorous finite difference solution of the two-dimensional boundary layer equations in the region close to the wall. However, this device greatly enhances the numerical solution efficiency since wider grid spacings can be used. Moreover, by arranging the region of Couette flow very close to the wall, the error due to this approximation may be rendered acceptable.

C. RESULTS AND DISCUSSION

Of the numerous results that were generated by GENMIX we focus attention here on those which especially pertain to the mechanism of silicon vapor deposition and/or help us improve the performance of a given silicon reactor.

1. Cross-Stream Profiles

The structure of the developing, turbulent flow in the "downstream" section is characterized by the velocity, temperature, and silicon mass fraction profiles across the reactor tube radius. Figure 2 shows the variations in normalized (with respect to the centerline values) velocity, temperature, and concentration vs the normalized radial distance from the pipe centerline. The operating conditions and pipe geometry were chosen to match the Westinghouse reactor design.[1] As expected from the prescribed mixing length distribution discussed earlier, it is possible to discern at least three regions of distinctly different behavior. Near the pipe centerline ($r/R = 0$) the fully turbulent core flow tends to even out all gradients due to rapid mixing. On the other hand, near the wall ($r/R = 1$) the steepest gradients are established under the influence of the molecular diffusivities for momentum, heat, and mass competing with residual (damped) turbulent diffusivities. Within this "viscous sublayer" the turbulent fluctuations decay rapidly (according to the Van Driest hypothesis) as the wall is approached. Thus, in the immediate vicinity of the wall, the final deposition of silicon may occur primarily by molecular mechanisms (i.e., a nearly laminar flow condition). Joining these two extremes is the outer turbulent (defect law) layer where transport occurs mainly due to diffusive turbulent fluctuations, characterized by a mixing length that varies linearly with distance from the wall. Note

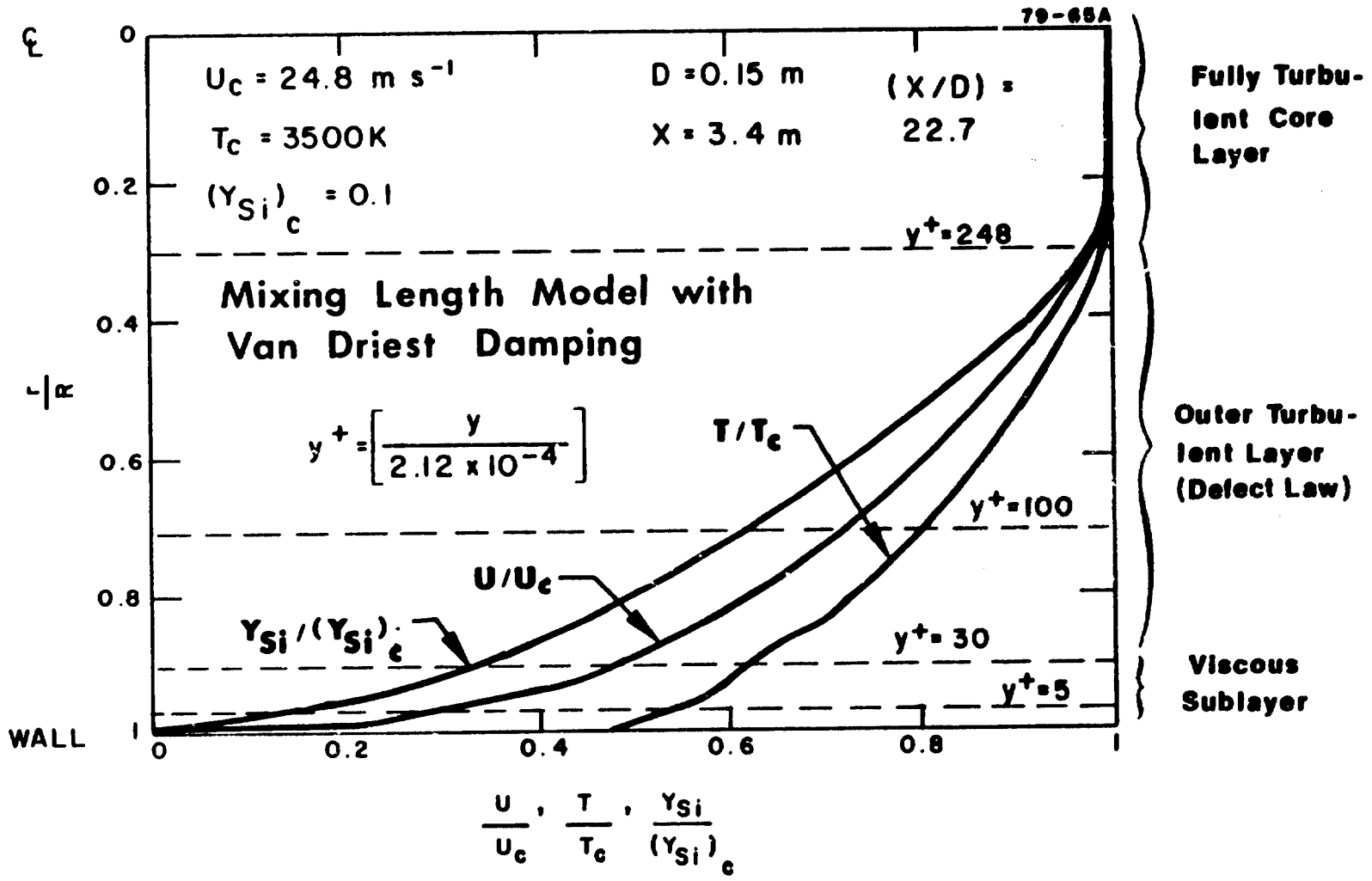

FIGURE 2. COMPUTED CROSS-STREAM PROFILES IN THE DEVELOPING, TURBULENT REACTOR FLOW

that in this region, unlike the viscous sublayer, there is negligible damping due to viscosity. Rather, the length and velocity scales of turbulence are smaller than in the core flow.

Although in reality the abovementioned zones blend continuously into each other, it has been customary to view turbulent pipe flows in terms of at least three different layers (with respect to the velocity profile)[16]: the laminar sublayer, the buffer layer, and the fully turbulent layer. Such a model is especially true of fully developed pipe flows. However, even Fig. 2 (for a developing flow) reveals these zones. The profiles are nearly linear next to the wall, implying that the laminar sublayer is a region of constant fluxes of momentum, heat, and mass. It is also interesting to note that the thicknesses of these three laminar sublayers are different, with the temperature and mass fraction layer thickness being equal and larger than the velocity layer thickness. Such a behavior is dictated by the input values of the laminar Prandtl and Schmidt numbers. In this case Pr = Sc = 0.7 was used. On the other hand, the buffer layer region is also seen to be one of nearly constant fluxes, even though the fluxes here are less than those in the laminar sublayer. Based on the prevailing wall shear stress, these two zones are expected to correspond to regions of the velocity profile that lie in the ranges $0 \leq y^+ \leq 5$ (laminar sublayer) and $5 < y^+ \leq 30$ (buffer layer). Both these zones fall within the viscous sublayer. Elsewhere in the boundary layer, the fluxes decrease with distance away from the wall and the final boundary layer thicknesses are nearly all equal. This is a consequence of the assumption that the effective Lewis and Prandtl numbers are nearly unity.

2. Streamwise Variation of Fluxes

Figure 3 shows the variation of the non-dimensional momentum, heat, and mass fluxes along the reactor length, X (non-dimensionalized with respect to the reactor diameter, D). The flow and other conditions are identical to those used for Fig. 2. The following definitions of the Stanton numbers for heat (St_h) and mass (St_m) transfer, and the skin-friction coefficient (C_f), were employed:

$$St_h \equiv - \frac{\dot{q}''_w}{\rho_b U_b (\tilde{h}_b - \tilde{h}_w)}$$

$$St_m \equiv - \frac{j''_w}{\rho_b U_b (Y_{i_b} - Y_{i_w})}$$

$$C_f \equiv \frac{\tau_w}{\frac{1}{2} \rho_b U_b^2}$$

where the subscript "b" refers to bulk (average) quantities and "w" refers to quantities evaluated at the reactor wall. $\tilde{h}$ is the stagnation enthalpy which may be defined in terms of the temperature and flow velocity as

$$\tilde{h} \equiv C_p T + \frac{u^2}{2}$$

In the present analysis $St_h = St_m$ due to the assumption of unity effective Lewis number. Furthermore, the closeness of the St and $C_f/2$ curves in Fig. 3

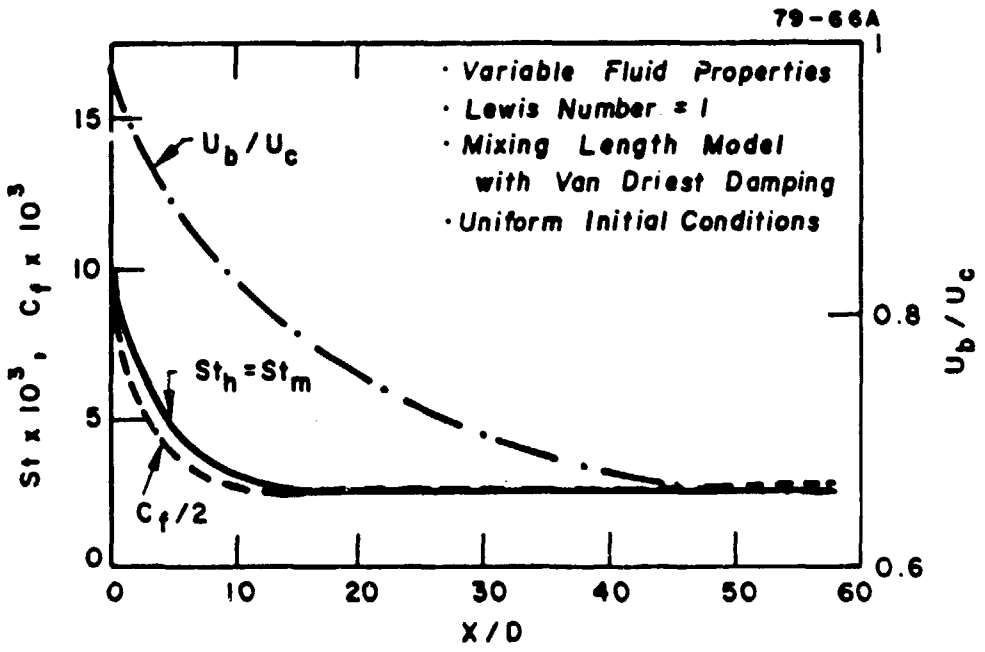

FIGURE 3. COMPUTED STREAMWISE VARIATION OF HEAT, MASS, AND MOMENTUM FLUXES TO THE REACTOR WALLS

suggests that under these conditions a Reynolds analogy of the type:

$$St \tilde{=} C_f/2$$

might be valid within the reactor since the effective Prandtl (and Schmidt) numbers are close to unity and the pressure variation in the downstream direction is small due to a low inlet velocity (in this case $U_{c,inlet} = 20$ m s^{-1}). In the other cases studied, it was found that greater deviations from this Reynolds analogy occurred with increasing inlet velocity due to more significant pressure gradients. Table I summarizes some of these results. It should be pointed out that "bulk" values of properties differ from their corresponding centerline values (denoted by the subscript "c"). This is clear from the variation of U_c/U_b with downstream distance. Typically, the centerline values monotonically exceed the bulk values in the region of developing flow and become constant only when "fully developed" flow conditions are established.*

---

* It has been shown[9] that in a pipe, as the developing shear layers merge, U_c exceeds $(U_c)_{fully\ developed}$ prior to settling down to a state of equality. Such details of shear layer interaction, however, cannot be predicted by the present mixing length model.

TABLE I

NON-DIMENSIONAL FLUXES

$U_{c,inlet} = 20\ m\ s^{-1}$

X/D	$C_{f/2}$	$St_h (= St_m)$	$Nu_h (= Nu_m)^a$	$Re_b{}^b$	$U_c/U_b{}^c$
2.5000E-03	8.3427E-02	1.1552E-01	3.5594E+02	4.4018E+03	1.0008E+00
2.5004E-01	1.1321E-02	1.2953E-02	4.0070E+01	4.4191E+03	1.0188E+00
2.7492E+00	4.7148E-03	5.1492E-03	1.5839E+01	4.3943E+03	1.0781E+00
5.2479E+00	4.0373E-03	4.3114E-03	1.3119E+01	4.3468E+03	1.1201E+00
7.7466E+00	3.6458E-03	3.8325E-03	1.1549E+01	4.3048E+03	1.1567E+00
1.0245E+01	3.4007E-03	3.5314E-03	1.0543E+01	4.2650E+03	1.1903E+00
1.2744E+01	3.2230E-03	3.3122E-03	9.8011E+00	4.2273E+03	1.2219E+00
1.5243E+01	3.0874E-03	3.1455E-03	9.2280E+00	4.1910E+03	1.2520E+00
1.7742E+01	2.9807E-03	3.0147E-03	8.7699E+00	4.1558E+03	1.2810E+00
2.0241E+01	2.8945E-03	2.9094E-03	8.3941E+00	4.1217E+03	1.3091E+00
2.2740E+01	2.8237E-03	2.8232E-03	8.0798E+00	4.0885E+03	1.3365E+00
2.5239E+01	2.7646E-03	2.7516E-03	7.8132E+00	4.0565E+03	1.3633E+00
2.7738E+01	2.7146E-03	2.6916E-03	7.5856E+00	4.0261E+03	1.3895E+00
3.0237E+01	2.6726E-03	2.6415E-03	7.3936E+00	3.9985E+03	1.4151E+00
3.2736E+01	2.6369E-03	2.5995E-03	7.2345E+00	3.9758E+03	1.4395E+00
3.5235E+01	2.6058E-03	2.5638E-03	7.1107E+00	3.9621E+03	1.4621E+00
3.7734E+01	2.5807E-03	2.5352E-03	7.0416E+00	3.9679E+03	1.4800E+00
4.0233E+01	2.5590E-03	2.5100E-03	7.0139E+00	3.9920E+03	1.4926E+00
4.2732E+01	2.5397E-03	2.4875E-03	7.0170E+00	4.0298E+03	1.5009E+00
4.5231E+01	2.5227E-03	2.4675E-03	7.0405E+00	4.0761E+03	1.5059E+00
4.7731E+01	2.5075E-03	2.4496E-03	7.0768E+00	4.1271E+03	1.5087E+00
5.0230E+01	2.4939E-03	2.4334E-03	7.1205E+00	4.1801E+03	1.5101E+00
5.2729E+01	2.4817E-03	2.4188E-03	7.1682E+00	4.2337E+03	1.5106E+00
5.5228E+01	2.4708E-03	2.4053E-03	7.2184E+00	4.2871E+03	1.5106E+00
5.7727E+01	2.4609E-03	2.3930E-03	7.2703E+00	4.3402E+03	1.5102E+00
6.0000E+01	2.4522E-03	2.3832E-03	7.3196E+00	4.3876E+03	1.5096E+00

[a] Nu is the Nusselt number.

[b] Re_b is the bulk Reynolds number based on pipe diameter.

[c] U_c/U_b is the ratio of centerline to bulk velocity.

TABLE I (Continued)

$U_{c,inlet} = 50\ m\ s^{-1}$

X/D	$C_{f/2}$	$St_h (= St_m)$	$Nu_h (= Nu_m)^a$	$Re_b{}^b$	$U_c/U_b{}^c$
2.5000E-03	3.6930E-02	5.2027E-02	4.0096E+02	1.1010E+04	1.0003E+00
2.5004E-01	6.7661E-03	7.9653E-03	6.1594E+01	1.1047E+04	1.0106E+00
2.7491E+00	3.2103E-03	3.6452E-03	2.7992E+01	1.0970E+04	1.0495E+00
5.2480E+00	2.7381E-03	3.0468E-03	2.3198E+01	1.0877E+04	1.0783E+00
7.7471E+00	2.4685E-03	2.7058E-03	2.0449E+01	1.0797E+04	1.1035E+00
1.0246E+01	2.2893E-03	2.4799E-03	1.8616E+01	1.0724E+04	1.1265E+00
1.2745E+01	2.1596E-03	2.3170E-03	1.7283E+01	1.0656E+04	1.1479E+00
1.5245E+01	2.0606E-03	2.1928E-03	1.6258E+01	1.0592E+04	1.1683E+00
1.7744E+01	1.9821E-03	2.0945E-03	1.5438E+01	1.0530E+04	1.1877E+00
2.0243E+01	1.9182E-03	2.0146E-03	1.4765E+01	1.0470E+04	1.2065E+00
2.2743E+01	1.8651E-03	1.9483E-03	1.4199E+01	1.0411E+04	1.2248E+00
2.5242E+01	1.8205E-03	1.8931E-03	1.3721E+01	1.0354E+04	1.2426E+00
2.7741E+01	1.7830E-03	1.8469E-03	1.3313E+01	1.0297E+04	1.2600E+00
3.0241E+01	1.7510E-03	1.8077E-03	1.2960E+01	1.0242E+04	1.2771E+00
3.2740E+01	1.7234E-03	1.7741E-03	1.2650E+01	1.0186E+04	1.2940E+00
3.5239E+01	1.6995E-03	1.7452E-03	1.2377E+01	1.0131E+04	1.3107E+00
3.7739E+01	1.6786E-03	1.7202E-03	1.2134E+01	1.0077E+04	1.3272E+00
4.0238E+01	1.6604E-03	1.6985E-03	1.1917E+01	1.0023E+04	1.3436E+00
4.2737E+01	1.6444E-03	1.6797E-03	1.1723E+01	9.9699E+03	1.3598E+00
4.5237E+01	1.6304E-03	1.6636E-03	1.1552E+01	9.9200E+03	1.3758E+00
4.7736E+01	1.6183E-03	1.6497E-03	1.1413E+01	9.8831E+03	1.3909E+00
5.0235E+01	1.6071E-03	1.6376E-03	1.1354E+01	9.9048E+03	1.4007E+00
5.2735E+01	1.5985E-03	1.6286E-03	1.1356E+01	9.9609E+03	1.4068E+00
5.5234E+01	1.5911E-03	1.6206E-03	1.1397E+01	1.0047E+04	1.4095E+00
5.7733E+01	1.5842E-03	1.6129E-03	1.1440E+01	1.0133E+04	1.4113E+00
6.0000E+01	1.5738E-03	1.6071E-03	1.1483E+01	1.0208E+04	1.4126E+00

TABLE I (Continued)

$U_{c,inlet} = 100\ m\ s^{-1}$

X/D	$C_{f/2}$	$St_h (= St_m)$	$Nu_h (= Nu_m)^a$	Re_b^b	U_c/U_b^c
2.5000E-03	1.9136E-02	2.7157E-02	4.1865E+02	2.2023E+04	1.0002E+00
2.5006E-01	4.3963E-03	1.7131E-03	2.6536E+01	2.2128E+04	1.0069E+00
2.7511E+00	2.0307E-03	9.9197E-04	1.5496E+01	2.2316E+04	1.0305E+00
5.2513E+00	1.8244E-03	9.0956E-04	1.4227E+01	2.2345E+04	1.0485E+00
7.7513E+00	1.6919E-03	8.5500E-04	1.3381E+01	2.2358E+04	1.0547E+00
1.0251E+01	1.5985E-03	8.1594E-04	1.2772E+01	2.2361E+04	1.0797E+00
1.2751E+01	1.5281E-03	7.8576E-04	1.2298E+01	2.2358E+04	1.0938E+00
1.5251E+01	1.4724E-03	7.6174E-04	1.1917E+01	2.2350E+04	1.1073E+00
1.7751E+01	1.4273E-03	7.4204E-04	1.1603E+01	2.2337E+04	1.1201E+00
2.0251E+01	1.3899E-03	7.2546E-04	1.1335E+01	2.2320E+04	1.1326E+00
2.2751E+01	1.3583E-03	7.1135E-04	1.1104E+01	2.2300E+04	1.1447E+00
2.5251E+01	1.3312E-03	6.9919E-04	1.0903E+01	2.2277E+04	1.1565E+00
2.7751E+01	1.3080E-03	6.8867E-04	1.0726E+01	2.2250E+04	1.1680E+00
3.0251E+01	1.2880E-03	6.7972E-04	1.0573E+01	2.2220E+04	1.1794E+00
3.2750E+01	1.2710E-03	6.7185E-04	1.0435E+01	2.2188E+04	1.1905E+00
3.5250E+01	1.2561E-03	6.6507E-04	1.0313E+01	2.2153E+04	1.2015E+00
3.7750E+01	1.2432E-03	6.5904E-04	1.0202E+01	2.2115E+04	1.2124E+00
4.0250E+01	1.2319E-03	6.5370E-04	1.0102E+01	2.2076E+04	1.2232E+00
4.2750E+01	1.2220E-03	6.4889E-04	1.0009E+01	2.2034E+04	1.2339E+00
4.5249E+01	1.2132E-03	6.4477E-04	9.9252E+00	2.1991E+04	1.2445E+00
4.7749E+01	1.2055E-03	6.4121E-04	9.8500E+00	2.1945E+04	1.2551E+00
5.0249E+01	1.1988E-03	6.3794E-04	9.7786E+00	2.1898E+04	1.2656E+00
5.2749E+01	1.1930E-03	6.3530E-04	9.7158E+00	2.1848E+04	1.2761E+00
5.5248E+01	1.1876E-03	6.3323E-04	9.6679E+00	2.1811E+04	1.2858E+00
5.7748E+01	1.1804E-03	6.3460E-04	9.6935E+00	2.1819E+04	1.2918E+00
6.0000E+01	1.1243E-03	9.3209E-04	1.4275E+01	2.1860E+04	1.2939E+00

TABLE I (Continued)

$U_{c,inlet}$ = 200 m s^{-1}:

X/D	$C_{f/2}$	$St_h (= St_m)$	$Nu_h (= Nu_m)^a$	$Re_b{}^b$	$U_c/U_b{}^c$
2.5000E-03	9.7242E-03	3.5939E-03	1.1082E+02	4.4050E+04	1.0001E+00
2.4996E-01	6.4262E-03	8.5827E-03	2.6380E+02	4.3909E+04	1.0061E+00
2.7489E+00	2.6766E-03	3.0626E-03	9.3320E+01	4.3530E+04	1.0392E+00
5.2480E+00	2.2268E-03	2.4864E-03	7.5214E+01	4.3215E+04	1.0630E+00
7.7473E+00	1.9831E-03	2.1798E-03	6.5547E+01	4.2957E+04	1.0834E+00
1.0247E+01	1.8267E-03	1.9845E-03	5.9356E+01	4.2727E+04	1.1019E+00
1.2746E+01	1.7221E-03	1.8600E-03	5.5350E+01	4.2512E+04	1.1191E+00
1.5245E+01	1.6467E-03	1.7649E-03	5.2266E+01	4.2307E+04	1.1354E+00
1.7745E+01	1.5995E-03	1.7083E-03	5.0348E+01	4.2105E+04	1.1512E+00
2.0244E+01	1.5919E-03	1.7019E-03	4.9907E+01	4.1892E+04	1.1667E+00
2.2743E+01	1.8083E-03	2.0271E-03	5.8935E+01	4.1533E+04	1.1838E+00
2.5241E+01	1.8984E-03	2.1609E-03	6.1671E+01	4.0778E+04	1.2064E+00
2.7740E+01	1.7884E-03	2.0120E-03	5.6928E+01	4.0421E+04	1.2259E+00
3.0239E+01	1.7579E-03	1.9848E-03	5.5668E+01	4.0068E+04	1.2440E+00
3.2738E+01	1.7717E-03	2.0150E-03	5.6166E+01	3.9820E+04	1.2608E+00
3.5236E+01	1.7937E-03	2.0508E-03	5.8035E+01	4.0427E+04	1.2791E+00
3.7735E+01	1.8130E-03	2.0763E-03	6.0009E+01	4.1249E+04	1.2997E+00
4.0234E+01	1.8257E-03	2.0958E-03	6.1497E+01	4.1919E+04	1.3202E+00
4.2733E+01	1.8348E-03	2.1082E-03	6.2669E+01	4.2467E+04	1.3366E+00
4.5232E+01	1.8419E-03	2.1178E-03	6.3652E+01	4.2937E+04	1.3529E+00
4.7731E+01	1.8474E-03	2.1254E-03	6.4507E+01	4.3358E+04	1.3703E+00
5.0230E+01	1.8520E-03	2.1318E-03	6.5281E+01	4.3747E+04	1.3885E+00
5.2729E+01	1.8581E-03	2.1432E-03	6.6179E+01	4.4112E+04	1.4071E+00
5.5228E+01	1.8652E-03	2.1532E-03	6.7017E+01	4.4464E+04	1.4261E+00
5.7727E+01	1.8733E-03	2.1641E-03	6.7880E+01	4.4809E+04	1.4453E+00
6.0000E+01	1.8799E-03	2.1737E-03	6.8647E+01	4.5116E+04	1.4647E+00

TABLE I (Continued)

$U_{c,inlet} = 400\ m\ s^{-1}$

X/D	$C_{f/2}$	$St_h (= St_m)$	$Nu_h (= Nu_m)^a$	Re_b^b	U_c/U_b^c
2.5000E-03	1.0918E-02	1.4835E-02	9.1491E+02	8.8103E+04	1.0000E+00
2.4995E-01	5.1554E-03	6.1955E-03	3.8037E+02	8.7705E+04	1.0070E+00
2.7488E+00	2.9634E-03	3.4991E-03	2.1241E+02	8.6720E+04	1.0402E+00
5.2473E+00	2.8199E-03	3.3404E-03	2.0011E+02	8.5579E+04	1.0692E+00
7.7457E+00	2.7730E-03	3.2953E-03	1.9674E+02	8.4424E+04	1.0975E+00
1.0244E+01	2.7626E-03	3.2941E-03	1.9196E+02	8.3250E+04	1.1258E+00
1.2743E+01	2.7586E-03	3.2991E-03	1.8955E+02	8.2079E+04	1.1543E+00
1.5241E+01	2.7605E-03	3.3111E-03	1.8754E+02	8.0915E+04	1.1831E+00
1.7739E+01	2.7681E-03	3.3311E-03	1.8598E+02	7.9757E+04	1.2122E+00
2.0238E+01	2.7807E-03	3.3583E-03	1.8494E+02	7.8672E+04	1.2413E+00
2.2736E+01	2.7982E-03	3.3929E-03	1.8715E+02	7.8800E+04	1.2593E+00
2.5234E+01	2.8020E-03	3.4042E-03	1.9155E+02	8.0386E+04	1.2992E+00
2.7733E+01	2.7930E-03	3.3965E-03	1.9502E+02	8.2026E+04	1.3393E+00
3.0231E+01	2.7800E-03	3.3827E-03	1.9769E+02	8.3485E+04	1.3518E+00
3.2730E+01	2.7656E-03	3.3664E-03	1.9985E+02	8.4811E+04	1.3490E+00
3.5228E+01	2.7507E-03	3.3490E-03	2.0172E+02	8.6048E+04	1.3469E+00
3.7727E+01	2.7358E-03	3.3311E-03	2.0339E+02	8.7228E+04	1.3451E+00
4.0226E+01	2.7211E-03	3.3130E-03	2.0493E+02	8.8367E+04	1.3436E+00
4.2724E+01	2.7067E-03	3.2951E-03	2.0638E+02	8.9475E+04	1.3422E+00
4.5223E+01	2.6926E-03	3.2774E-03	2.0776E+02	9.0560E+04	1.3409E+00
4.7722E+01	2.6789E-03	3.2600E-03	2.0909E+02	9.1624E+04	1.3396E+00
5.0221E+01	2.6655E-03	3.2430E-03	2.1037E+02	9.2671E+04	1.3385E+00
5.2719E+01	2.6526E-03	3.2264E-03	2.1162E+02	9.3701E+04	1.3374E+00
5.5218E+01	2.6400E-03	3.2101E-03	2.1283E+02	9.4715E+04	1.3363E+00
5.7717E+01	2.6277E-03	3.1943E-03	2.1402E+02	9.5715E+04	1.3352E+00
6.0000E+01	2.6141E-03	3.2032E-03	2.1662E+02	9.6609E+04	1.3343E+00

3. Silicon Collection Efficiency

The ratio of the mass of silicon deposited on the reactor walls, due to the boundary layer convective-diffusion processes, to the total mass of silicon entering a given reactor may be defined as the "collection efficiency." This ratio can readily be calculated by integrating the downstream variation of the silicon mass flux to the walls, j''_w, over the reactor length of interest. Figure 4 shows the results of such a computation. It is seen that the silicon collection efficiency, for a given inlet flow velocity, increases as the reactor length increases. Initially, this increase is slower than in the aft regions (as expected from the mass flux variation shown in Fig. 3). Furthermore, Fig. 4 reveals the important effect of changing flow residence times on the reactor's performance. As expected, faster through-flows reduce the collection efficiency drastically since the flow time is much less than the time for effective silicon vapor diffusion to the reactor walls. Charts of this type can help the designer produce an "optimum reactor," at least from the standpoint of silicon separation and collection.

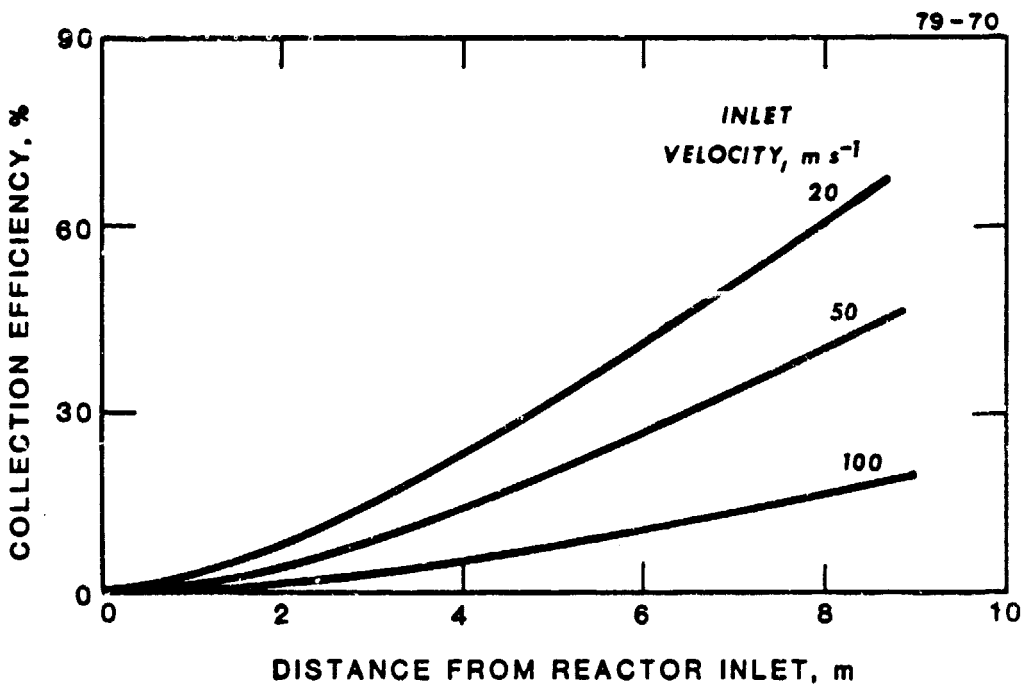

FIGURE 4. COMPUTED VARIATION OF SILICON VAPOR COLLECTION EFFICIENCY OF A REACTOR WITH LENGTH AND INLET VELOCITY

IV. SILICON COLLECTION VIA JET IMPINGEMENT

The new AeroChem $SiCl_4$/Na reactor[2] will employ a considerably different Si collection scheme from that used by Westinghouse.[1] In this new reactor a jet impingement method of collecting Si(ℓ) droplets will be tested. It is expected that this collection method will be effective in collecting the very small Si(ℓ) droplets produced via the $SiCl_4$/Na reaction and in effectively separating the Si(ℓ) from the NaCl produced by the reaction. The reactor and Si collection crucible to be tested shortly are shown in Fig. 5. Na(g) and $SiCl_4$(g) react in a graphite chamber, 8 cm in diam and 16 cm long. The reaction temperature can be adjusted by heating the reactor, and initial tests will be done with $\approx$ 1700 K walls; the gas within the reactor is expected to be at $\gtrsim$ 2300 K. Flow rates of reactants will be adjusted to maintain a pressure of 0.5 atm (360 Torr). At the bottom of the reactor a simple converging nozzle with a throat diameter of 1.2 cm will allow the reacted NaCl(g)/Si(ℓ) droplet mixture to exhaust into a large vacuum vessel held at a pressure (for initial testing) of $\approx$10 Torr. (Since the products of reaction are condensible and only a very small amount of Ar is used to keep the $SiCl_4$ delivery line shielded from the hot product gases only a very small pumping capacity is required after the initial pumpdown.) The jet of product gas/droplets will impinge on an Si(ℓ) surface at the heated crucible. This will result in a normal shock standing above the Si(ℓ) surface and in a post-shock layer at high temperature and moderate pressure through which the droplets must pass to reach the surface. Using standard isentropic flow and normal shock tables and the operating conditions given above, the values of pressure, temperature, density, and gas velocity in the reactor, the jet and the post-shock layer given in Table II are obtained.

Calculations have been done to find the minimum Si droplet size which might be expected to penetrate the post-shock layer and impinge on the surface, i.e., be collected by impingement. The first step in the calculation is to find the post-shock layer thickness. To do this one assumes that the thickness is uniform and determined by the fact that the radial mass flow beneath the shock must be equal to the mass flow of gas in the jet. One thus has, for the post-shock thickness, ℓ_{sh},

$$\ell_{sh} = 1/2\ \rho_j u_j r_j / (u_s \rho_s)$$

79-61

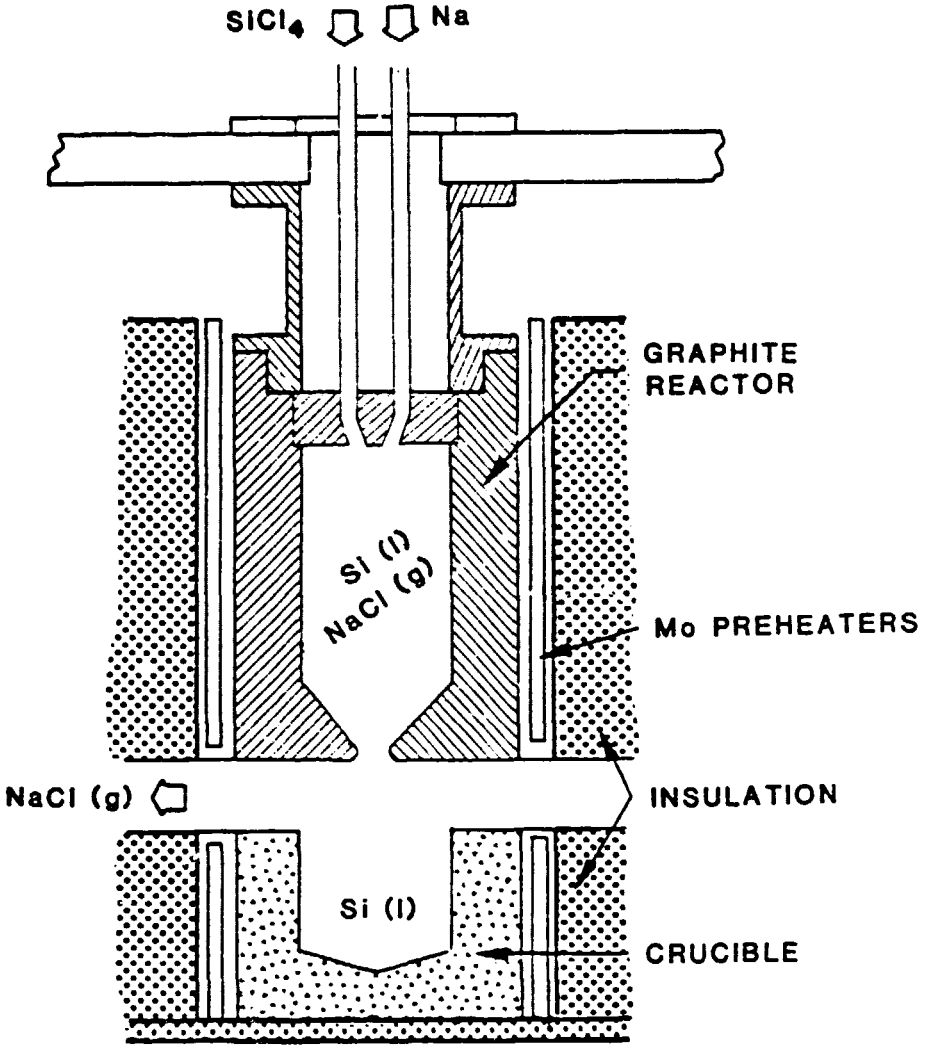

FIGURE 5. AEROCHEM GRAPHITE REACTOR WITH Si COLLECTION CRUCIBLE

TABLE II

TENTATIVE OPERATING CONDITIONS FOR THE AEROCHEM REACTOR

	Reactor	Jet	Post-Shock Layer
Pressure, Torr	360	9.5	110
Temperature, K	2300	810	2180
Density, gm ml^{-1}	1.37(-4)	1.00(-5)	4.0(-5)
Velocity, cm s^{-1}	0	1.36(5)	3.3(4)
Mach No.	0	3.02	0.47

where ρ is density, u is velocity, and the subscripts j and s refer to the jet and post-shock regions. The radius of the jet, r_j, is 2.07 times the exit radius of the nozzle, or 2.5 cm. Using the values for density and velocities, of Table II, we find

$$\ell_{sh} = 1.3 \text{ cm}$$

The calculation of stopping distances for droplets entering the post-shock layer poses a major problem. Values for stopping distances calculated two ways are given in Table III. A glance at this table reveals that the Knudsen numbers, N_{Kn}, (the ratio of molecular mean free path to droplet radius) for the very small droplets of interest (diam · 0.5 μm) are very large. This raises a problem since the usual Stokes relationship for computing stopping, S_{st}, even with corrections for molecular slip, will not be trustworthy for such large values of N_{Kn}. This standard relationship is the formula based on Stokes flow:

$$S_{st} = \frac{\rho_p d_p^2 u_j}{18 \mu_s} \times SCF$$

where μ_s is the viscosity of the post-shock gas, $\mu_s = 1.1 \times 10^{-3}$ g $s^{-1}cm^{-1}$,

TABLE III

STOPPING DISTANCES FOR DROPLETS ENTERING THE POST-SHOCK LAYER

Layer thickness = 1.3 cm

Droplet Diam, μm	Knudsen No.	Stokes Stopping Distance, cm	Stopping Distance, based on Molecular Collisions, cm
0.01	1220	0.04	0.03
0.05	240	0.19	0.58
0.10	120	0.39	1.57
0.50	24	2.0	12.4

ρ_p and d_p are the droplet density (2.4 g ml^{-1}) and diameter, respectively, and the Stokes-Cunningham slip factor is

$$SCF = 1 + 1.26\ N_{Kn} + 0.4\ N_{Kn}\ \exp(-1.1/N_{Kn})$$

Table III includes values for S_{st} obtained using this formula. Physically, the trouble with such a formula is the assumption that a particle, as it moves through the gas, carries with it an enveloping cloud (boundary layer) of gas with it. For $N_{Kn} >> 10$ this will not be the case and a better approach would be one in which particle kinetic energy losses result from individual particle/gas molecule collisions assuming that the gas molecules in front of the oncoming particle are not disturbed by the particle's approach (i.e., a "free-molecule" approach rather than a "continuum" approach).

If E_p is the kinetic energy of a particle of mass m_p, then the loss of kinetic energy suffered by collision with a single gas molecule of mass m_g (considered on the average to be stationary) will be (with averaging performed over the surface of the particle)

$$\Delta E_p = -2\ m_g E_p / m_p$$

The number of such collisions suffered per cm of travel will be $(\pi d_p^2 n_g)/4$ where n_g is the number of gas molecules per ml. The collisional stopping distance S_{coll} is then given by

$$S_{coll} = \left(\int_{E_p^i}^{E_p^f} \frac{d E_p}{E_p} \right) \times \frac{2 m_g}{\pi d_p^2 n_g m_p}$$

where $E_p^i (= 1/2\ m_p u_j^2)$ is the particle kinetic energy as it enters the post-shock layer and E_p^f is the final particle kinetic energy. The values of E_p^f specified cannot be zero and for Table III have been taken to be

$$E_p^f = 1.0 \times 10^4\ k\ T_s$$

i.e., 6700 times the mean thermal translational energy of gas molecules at the post-shock temperature. Fortunately, the calculation does not depend strongly on the choice of E_p^f; a change of a factor of 10 in its value changes the values of S_{coll} by a factor of 2.3, (i.e., ln 10).

From Table III it is seen that $S_{coll} > \ell_{sh}$ for $d_p = 0.1$ μm. Even if the Stokes stopping distance S_{st} is picked as a conservative value it is found that droplets with $d_p = 0.3$ μm will reach the liquid surface by impingement. Thus it is found that the jet impingement method is capable of collecting very small droplets and, if such droplets are produced, Si collection efficiencies will be high. The sizes of droplets expected will shortly be examined using the modified LAPP code now in its final testing stages and operating conditions will be sought which will yield drops with $d_p \gtrsim 0.1$ μm.

V. CONCLUSIONS

A model and computer code have been developed to describe the behavior of the turbulent, developing boundary layer flow in the "downstream" section of a tubular reactor, where the crucial silicon separation/collection is affected. The present analysis necessitated modification of the GENMIX-4A code[3] in order to achieve solutions to the coupled system of parabolic, partial differential equations for conservation of overall mass, momentum, energy, and species. The

turbulence model adopted was of the mixing-length type, with wall damping according to a modified Van Driest hypothesis. In particular, the following objectives have been achieved:

(i) Silicon vapor deposition processes can now be analyzed with due regard to the structure of the developing turbulent flow that prevails over most of a reactor's length.

(ii) The modified GENMIX code now provides a computational capability that should be useful to the designer in optimizing a given reactor, with a minimum of experimentation.

(iii) A reliable basis for assessing the silicon vapor collection efficiency of a given reactor has been established.

Finally, it must be mentioned that Soret transport of silicon vapor was intentionally excluded from this analysis, since it is expected to be small in the absence of condensation. The effect, however, will become important when silicon droplets are considered in future analyses.[6-8,17]

Calculations have also been performed which indicate that the "jet impingement" Si collection method to be used with the new AeroChem $SiCl_4$/Na reactor is capable of collecting very small Si droplets.

VI. PLANS

During the next quarter, boundary layer calculations which will include Si condensation and thermophoretic droplet deposition[3] on the reactor walls will be made to more accurately determine Si collection efficiencies for the Westinghouse reactor, under a variety of operating conditions. The modified LAPP code will be used to predict Si droplet size distributions in both the Westinghouse and AeroChem reactors.

VII. NEW TECHNOLOGY

No reportable items of new technology have been identified.

VIII. REFERENCES

1. Fey, M.G., "Development of a Process for High Capacity Arc Heater Production of Silicon for Solar Arrays," Westinghouse Electric Corp., Quarterly Report, DOE/JPL 954589, April-June 1978.

2. Olson, D.B. and Gould, R.K., "Silicon Halide-Alkali Metal Flames as a Source of Solar Grade Silicon," Seventh Quarterly Report, AeroChem TN-205, DOE/JPL 954777-79/7.

3. Patankar, S.V. and Spalding, D.B., Heat and Mass Transfer in Boundary Layers (Intertext Books, London, 1970).

4. Boelter, L.M.K., Young, G., and Iverson, E.W., "An Investigation of Aircraft Heaters - Distribution of Heat Transfer Rate in the Entrance Section of a Circular Tube," NASA TN-1451, July 1948.

5. Srivastava, R. and Gould, R.K., "Development of a Model and Computer Code to Describe Solar Grade Silicon Production Processes," Fifth Quarterly Report, AeroChem TN-202, DOE/JPL 954862-79/5, February 1979.

6. Srivastava, R. and Rosner, D.E., "A New Approach to the Correlation of Boundary Layer Mass Transfer Rates with Thermal Diffusion and/or Variable Properties," Int. J. Heat Mass Transfer (in press).

7. Srivastava, R. and Rosner, D.E., "Falsification of Particle Size Distribution for Capture by Simultaneous Brownian Motion and Thermophoresis," Int. J. Heat Mass Transfer (to be submitted).

8. Srivastava, R., "Modeling the Characteristics of High Purity Silicon Production Processes," (in preparation).

9. Launder, B.E., "Heat and Mass Transport," in Turbulence, Vol. 12, Topics in Applied Physics, P. Bradshaw, Ed. (Springer-Verlag, Berlin, 1976) Chap 6.

10. Stephenson, P.L., "A Theoretical Study of Heat Transfer in Two-Dimensional Turbulent Flow in a Circular Pipe and between Parallel and Diverging Plates," Int. J. Heat Mass Transfer 19, 413 (1976).

11. Bankston, C.A. and McEligot, D.M., "Turbulent and Laminar Transfer to Gases with Varying Properties in the Entry Region of Circular Ducts," Int. J. Heat Mass Transfer 13, 319 (1970).

12. Spalding, D.B., GENMIX: A General Computer Program for Two-Dimensional Parabolic Phenomena, HMT Series, Vol. 1 (Pergamon Press, New York, 1977).

13. Crawford, M.E. and Kays, W.M., "STAN-5, A Program for Numerical Computation of Two-Dimensional Internal/External Boundary Layer Flows," Thermosciences Div. Mechanical Engng. Dept., Stanford University, Report No. HMT-23, 1975.

14. Van Driest, E.R., "On Turbulent Flow Near a Wall," J. Aero. Sci. 23, 1007 (1956).

15. von Mises, R., "Bemerkungen zur Hydrodynamik," Z. Angew. Math. Mech. 7, 425 (1927).

16. von Karman, Th., "The Analogy between Fluid Friction and Heat Transfer," Trans. ASME 61, 705 (1939).

17. Srivastava, R. and Gould, R.K., "Rational Thermodynamic and Transport Property Schemes for Silicon Vapor and Particles," (in preparation).